

ChemComm

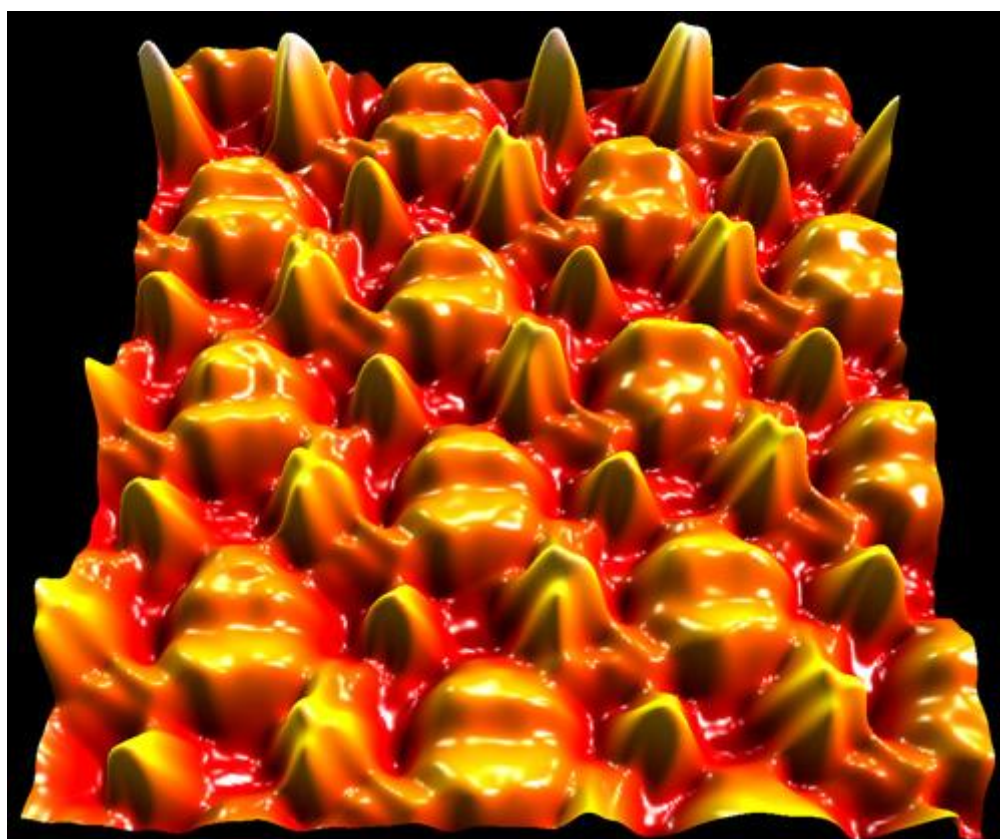
This article is part of the

Molecule-based Surface Chemistry web themed issue

Guest Editors include Steven De Feyter, Federico Rosei & Dmitrii Perepichka

Please visit the website to access the other articles in this issue:-

<http://www.rsc.org/chemcomm/surfacechemistry>



Cite this: *Chem. Commun.*, 2011, **47**, 9453–9455

www.rsc.org/chemcomm

Halogen bonds as stabilizing interactions in a chiral self-assembled molecular monolayer†‡

Rico Gutzler,^{*ab} Oleksandr Ivashenko,^a Chaoying Fu,^{ab} Jaelyn L. Brusso,^{§a} Federico Rosei^{*b} and Dmitrii F. Perepichka^{*a}

Received 26th May 2011, Accepted 5th July 2011

DOI: 10.1039/c1cc13114a

We report the formation of highly-ordered self-assembled monolayers of an achiral organic semiconductor molecule. STM results show spontaneous formation of very large single domains of ordered chiral monolayers. DFT calculations support the identification of halogen bonds as the primary interactions that steer molecular self-assembly, leading to organizational chirality.

Molecular self-assembly is a bottom-up approach in the design of supramolecular architectures suitable for various applications including functional materials and organic electronics.^{1–4} Weak molecular interactions like van der Waals forces,⁵ aromatic interactions,⁶ hydrogen bonding,^{7,8} metal coordination,⁹ and ionic interactions¹⁰ are the basis of these supramolecular architectures and the fundamental driving force in the crystallization of organic molecules.¹¹ A potential benefit of halogen bonding *versus* commonly encountered hydrogen bonding is that the C–X is not as easily ionizable as the X–H in hydrogen-bonded self-assembled molecular networks (SAMNs), making halogen bonded materials more advantageous in charge-transport applications.^{12,13} Furthermore, both halogen and hydrogen bonds can interact simultaneously with the same bond acceptor, enhancing binding and introducing new binding motifs for supramolecular chemistry.¹⁴

While halogen bonding has been used extensively in 3D crystal engineering,¹³ little is known about its application in surface-confined molecular self-assembly. Very recently, two-dimensional halogen bonded networks of tris(*p*-bromophenyl)benzene¹⁵ and dibromoanthraquinone¹⁶ were observed at the vacuum/metal interface. The latter provides a detailed description of the mechanisms of halogen bonding. The actual measured

Br⋯Br contacts, however, are not shorter than the sum of van der Waals radii, raising the question of how significant the specific contribution of halogen bonding is in these monolayers. At the solid–liquid interface, where the binding of molecules to the surface is weakened by interactions with the solvent, neither halogen bonding nor other weak interactions between heavy atoms have been yet observed to stir self-assembly. Octathiocirculene molecules, for example, do not self-assemble if not included into a host–guest matrix.¹⁷

Herein we present the first case of halogen bonding in monolayers at the liquid/solid interface using scanning tunneling microscopy (STM) to study the self-assembly of TBTTA (Fig. 1a), a tetrabrominated derivative of the known organic semiconductor tetrathienoanthracene.^{18–20} A drop of saturated solution of TBTTA in 1,2,4-trichlorobenzene (TCB) is applied to a freshly cleaved graphite surface. The molecules self-assemble from solution on the surface and form stable monolayers

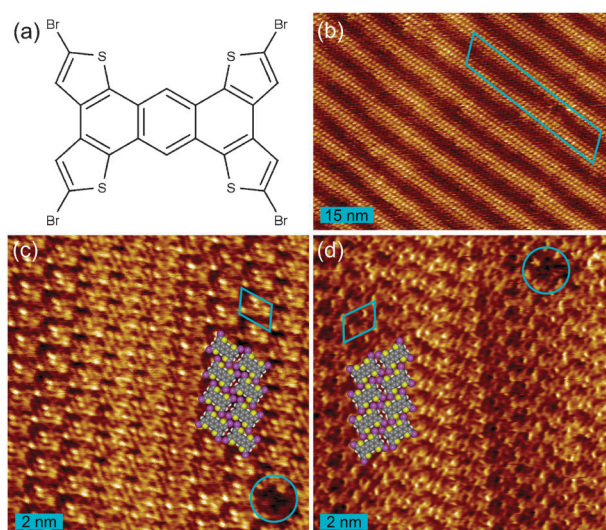


Fig. 1 (a) Chemical structure of TBTTA. (b) Overview STM topograph of the TBTTA monolayer at the 1,2,4-trichlorobenzene/graphite interface. The blue rectangle indicates the unit cell of the moiré pattern ($I_T = 100$ pA, $V_{\text{bias}} = 800$ mV). (c) Small-scale STM topograph of the TBTTA monolayer with a molecular model. The blue rectangle corresponds to the unit cell that contains one molecule. A single-molecule defect is encircled in blue ($I_T = 100$ pA, $V_{\text{bias}} = -800$ mV). (d) Enantiomeric counterpart to (c) ($I_T = 500$ pA, $V_{\text{bias}} = -300$ mV).

^a Department of Chemistry and Centre for Self-Assembled Chemical Structures, McGill University, 801 Sherbrooke Str. West, Montreal, QC H3A 2K6, Canada. E-mail: dmitrii.perepichka@mcgill.ca

^b Institut National de la Recherche Scientifique and Centre for Self-Assembled Chemical Structures, Université du Québec, 1650 boulevard Lionel-Boulet, Varennes, QC J3X 1S2, Canada.

E-mail: rosei@emt.inrs.ca, gutzler@emt.inrs.ca

† This article is part of the “Molecule-based surface chemistry” web-theme issue for ChemComm.

‡ Electronic supplementary information (ESI) available: Experimental and computational details, additional STM data, additional computational data. See DOI: 10.1039/c1cc13114a

§ Present address: Department of Chemistry, University of Ottawa, Ottawa, ON, Canada.

which are imaged by STM. We demonstrate that halogen bonding, a rather weak binding motif, is in fact strong enough to stabilize supramolecular monolayers under the equilibrium conditions of liquid/solid interfaces. We find exceptionally large domains that show organizational chirality, converting the achiral graphite surface in a chiral interface.

TBTTA is a planar D_{2h} -symmetric molecule with eight heavy atoms (S, Br) on its periphery. At the TCB/graphite interface, TBTTA assembles into a crystalline monolayer structure with an oblique unit cell ($a = 1.1$ nm, $b = 1.5$ nm, $\alpha = 66^\circ$, Fig. 1b and c) which contains one flat lying molecule. The high degree of molecular organization is also apparent from an unusually pronounced moiré pattern, a superperiodic structure caused by the interaction between the molecular lattice and the graphite surface (Fig. 1b and ESI†). Such interactions also lead to variations in the image contrast at the submolecular level, complicating the identification of individual molecules within the SAMN. We identified the molecular packing motif by analyzing the structure of void defects in the SAMN (Fig. 1 and ESI†). The molecules arrange in slip-stacked tapes (running nearly vertically in Fig. 1c and d) *via* Br \cdots S and Br \cdots H contacts. Laterally these tapes are held together by Br \cdots Br and Br \cdots H interactions in an overall close-packed arrangement. This packing motif leads to an interesting case of organizational chirality:²¹ while TBTTA itself is achiral, it forms chiral 2D crystalline domains. The binding conformation of TBTTA in an oblique unit cell of $p2$ symmetry necessarily leads to a chiral monolayer, and we have observed both enantiomers in different experimental runs (*cf.* Fig. 1c and d).

Another noteworthy feature rarely observed in SAMNs at the solid-liquid interface is the quick (within a few minutes) self-assembly of very large ($>1 \mu\text{m}^2$) single-crystalline domains (see ESI†). In our numerous experiments, no domain boundaries were ever observed within the same terrace of HOPG after equilibration. The fact that the monolayer is monocrystalline over large areas signifies that the achiral graphite surface is transformed into a chiral adlayer interface by physisorption of a monolayer of TBTTA. However, the SAMN is interrupted at the boundaries of graphite terraces (ESI†), which ultimately limits the size of the chiral domains.

To gain deeper insights into the intermolecular binding mechanisms within the monolayer we employed density functional theory (DFT) calculations using the M06-2X functional, which was shown to accurately model dispersive and other weak interactions,²² applying the 6-31G(d,p) basis set. The geometry-optimized unit cell ($a = 1.11$ nm,

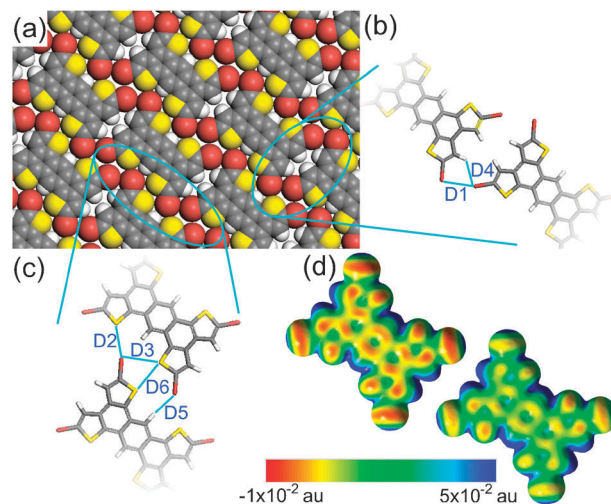


Fig. 2 (a) DFT optimized structure of TBTTA SAMN; intermolecular contacts along the (b) short side and (c) long side of the molecule. (d) ESP map of TBTTA in vacuum (left) and in SAMN (right).

$b = 1.42$ nm, $\alpha = 68^\circ$ angle, Fig. 2a) reproduces closely the structure of the observed TBTTA monolayer. The counterpoise corrected binding energy within the monolayer was found to be -3.1 kcal mol $^{-1}$ (ESI†). Fig. 2b and c disclose intermolecular contacts that are shorter than the sum of the respective van der Waals radii (see also Table 1). The four close contacts that are formed between two molecules along the long side of the molecules are one Br \cdots H bond D5, one S \cdots S D6 bond, and two Br \cdots S bonds D2 and D3 (Table 1). The second binding site is along the short side of the molecule and includes one Br \cdots Br and one Br \cdots H bond (D1 and D4, respectively). The Br \cdots Br distance (3.42 Å) is significantly shorter than twice the van-der-Waals radius of Br (3.70 Å) and is at the lower end of the 3.4–3.9 Å range found for Br \cdots Br contacts in organic crystals.^{23–25} The distance found in our SAMN lies at the lower end of this range.

In addition to the observed structure our calculations identified two other stable polymorphs. One is a symmetric achiral polymorph with a binding energy of -1.1 kcal mol $^{-1}$ (area of unit cell $A = 1.63$ nm 2 and energy per unit area $E = -1.1$ mcal m $^{-2}$). This structure does not provide optimal arrangement for favourable Br \cdots Br interactions (ESI†). The second polymorph, like the observed structure, is chiral. Although it optimizes the number of Br \cdots Br contacts and has a slightly larger binding energy of -3.2 kcal mol $^{-1}$, it is less stable in view of its lower packing density in the

Table 1 Close-contact distances D between two adjacent molecules

	$D/\text{Å}$	$\Sigma_{\text{vdw}}^b/\text{Å}$	Interacting orbitals	δ^c	$\Delta E^{(2)d}/\text{kcal mol}^{-1}$
D1 ^a Br \cdots Br	3.42	3.70	$n_{\text{Br}} \rightarrow \sigma_{\text{C-Br}}^*$	0.037	2.8
D2 Br \cdots S	3.64	3.65	$n_{\text{Br}} \rightarrow \sigma_{\text{C-S}}^*$	0.040	0.5
			$n_{\text{S}} \rightarrow \sigma_{\text{C-Br}}^*$	0.034	1.2
D3 Br \cdots S	3.41	3.65	$n_{\text{Br}} \rightarrow \sigma_{\text{C-S}}^*$	0.039	0.8
D4 Br \cdots H	2.95	3.05	$n_{\text{Br}} \rightarrow \sigma_{\text{C-H}}^*$	0.019	2.2
D5 Br \cdots H	2.86	3.05	$n_{\text{Br}} \rightarrow \sigma_{\text{C-H}}^*$	0.018	2.2
D6 S \cdots S	3.50	3.60	$n_{\text{S}} \rightarrow \sigma_{\text{C-S}}^*$	0.027	0.9

^a Labels as shown in Fig. 2. ^b The sum of the corresponding van-der-Waals radii. ^c Occupancy of the antibonding orbital. ^d Second-order perturbation energy lowering $\Delta E^{(2)}$.

monolayer ($A = 1.61 \text{ nm}^2$ and $E = -3.2 \text{ mcal m}^{-2}$). From the three predicted polymorphs, the binding energy per unit area favors the experimentally observed structure ($A = 1.47 \text{ nm}^2$ and $E = -3.5 \text{ mcal m}^{-2}$).

Analysis of the electrostatic potential (ESP) of TBTTA (Fig. 2d) offers an intuitive explanation for the observed self-assembly geometry. The ESP map reveals a charge distribution that is particularly noteworthy on the Br atoms: a negative equatorial ring (red) around the Br atoms is accompanied by a positive cap (blue) at the tip of the atom. Such polarization, referred to as a σ -hole, is responsible for the halogen...halogen bonding.²⁶ In our SAMN (Fig. 2), the electropositive cap of one bromine atom points towards the electronegative ring of a bromine atom on a neighbouring molecule, thus leading to an electrostatic attraction (D1 contact in Fig. 2c). The same bromine atom points with its negative ring towards an electropositive hydrogen atom in the Br...H D4 bond. This Br...Br...H triangular structure has been observed in 3D crystal structures of other halogenated molecules.^{24,25} The Br atom at the long side of TBTTA points with its electronegative ring towards the hydrogen (Br...H bond D5, Fig. 2b). In addition, the positive end cap of the bromine atom reaches out towards an electron lone pair on one S atom in the Br...S bond D2. The overall picture can be described by the tendency of the halogen atom to bind a nucleophile with its positive cap and an electrophile with its negative ring.

Comparing the ESP for the isolated molecule with that of molecules in the SAMN (Fig. 2d) demonstrates a non-negligible effect of packing on molecular polarization. The negative ring around the bromine atoms decreased in magnitude as does the negative potential at the sulfur atoms. Additionally, the symmetry of ESP on the molecule is broken in the monolayer due to different interaction environments for different parts of the molecule. The symmetry breaking from D_{2h} to C_{2h} in the SAMN is likewise reflected in the molecular orbitals (ESI†).

Natural bond orbital (NBO) analysis on the optimized geometry of the molecular layer yields many attractive contributions. Most notable is the second-order energy lowering $\Delta E^{(2)}$ in the Br...Br D1 and Br...H D4 bonds. The geometry of the D1 contact ($\text{C-Br1...Br2} = 96^\circ$, $\text{Br1...Br2-C} = 160^\circ$) enables weak donor-acceptor interactions of the lone pair orbital (n) of the Br1 atom with the σ^* orbital of the adjacent Br2-C bond. Also, the lone pair of Br2 donates charge to the σ^* orbital of H-C bond through the D4 contact (see Table 1). To a lesser extent, charge transfer from Br and S lone pairs into σ^* orbitals of adjacent molecules along the long side binding (D2, D3, D6) also stabilizes the supramolecular structure. Aside from dispersion and electrostatic forces, this donor-acceptor charge transfer is yet another non-negligible effect in the observed halogen bonding interactions.

Our study demonstrates the halogen...halogen bond as a new binding interaction in the self-assembly of molecular networks at the liquid/solid interface. The achiral TBTTA molecule forms chiral monolayers of exceptionally large domains at the micrometre scale, converting the achiral graphite surface into a chiral molecular interface. Compared to extensively studied H-bonding interactions, halogen bonding is weaker in energy which leads to faster dissociation dynamics.

Also, rigidity of haloaromatic building blocks reduces the unfavourable entropy of self-assembly, as compared to van der Waals binding motifs in aliphatic hydrocarbons. Together these factors accelerate crystal growth and Ostwald ripening, resulting in unusually quick formation of very large domains. Thus, SAMNs containing a large number of halogen interactions constitute a realistic route towards the formation of monocrystalline monolayers over large areas.

This work was supported by NSERC of Canada through Discovery Grants, by FQRNT (Team Grant) and MDEIE. We thank CERMM for access to computational infrastructure.

Notes and references

- 1 A. Ciesielski, C.-A. Palma, M. Bonini and P. Samorì, *Adv. Mater.*, 2010, **22**, 3506–3520.
- 2 F. Rosei, M. Schunack, Y. Naitoh, P. Jiang, A. Gourdon, E. Laegsgaard, I. Stensgaard, C. Joachim and F. Besenbacher, *Prog. Surf. Sci.*, 2003, **71**, 95–146.
- 3 J. A. A. W. Elemans and S. de Feyter, *Soft Matter*, 2009, **5**, 721–735.
- 4 J. E. Green, J. Wook Choi, A. Boukai, Y. Bunimovich, E. Johnston-Halperin, E. DeIonno, Y. Luo, B. A. Sheriff, K. Xu, Y. Shik Shin, H.-R. Tseng, J. F. Stoddart and J. R. Heath, *Nature*, 2007, **445**, 414–417.
- 5 K. S. Mali, K. Lava, K. Binnemans and S. De Feyter, *Chem.–Eur. J.*, 2010, **16**, 14447–14458.
- 6 R. Gutzler, S. Lappe, K. Mahata, M. Schmittel, W. M. Heckl and M. Lackinger, *Chem. Commun.*, 2009, 680–682.
- 7 K. G. Nath, O. Ivasenko, J. M. MacLeod, J. A. Miwa, J. D. Wuest, A. Nanci, D. F. Perepichka and F. Rosei, *J. Phys. Chem. C*, 2007, **111**, 16996–17007.
- 8 J. M. MacLeod, O. Ivasenko, C. Fu, T. Taerum, F. Rosei and D. F. Perepichka, *J. Am. Chem. Soc.*, 2009, **131**, 16844–16850.
- 9 M. Marschall, J. Reichert, A. Weber-Bargioni, K. Seufert, W. Auwaerter, S. Klyatskaya, G. Zoppellaro, M. Ruben and J. V. Barth, *Nat. Chem.*, 2010, **2**, 131–137.
- 10 B. A. Friesen, B. Wiggins, J. L. MacHale, U. Mazur and K. W. Hipps, *J. Phys. Chem. C*, 2011, **115**, 3990–3999.
- 11 L. Bartels, *Nat. Chem.*, 2010, **2**, 87–95.
- 12 M. L. Tang and Z. Bao, *Chem. Mater.*, 2011, **23**, 446–455.
- 13 M. Fourmigué and P. Batail, *Chem. Rev.*, 2004, **104**, 5379–5418.
- 14 A. R. Voth, P. Khuu, K. Oishi and P. S. Ho, *Nat. Chem.*, 2009, **1**, 74–79.
- 15 H. Walch, R. Gutzler, T. Sirtl, G. Eder and M. Lackinger, *J. Phys. Chem. C*, 2010, **114**, 12604–12609.
- 16 J. K. Yoon, W.-J. Son, K.-H. Chung, H. Kim, S. Han and S.-J. Kahng, *J. Phys. Chem. C*, 2011, **115**, 2297–2301.
- 17 O. Ivasenko, J. M. MacLeod, K. Y. Chernichenko, E. S. Balenkova, R. V. Shpanchenko, V. G. Nenajdenko, F. Rosei and D. F. Perepichka, *Chem. Commun.*, 2009, 1192–1194.
- 18 J. L. Brusso, O. D. Hirst, A. Davdand, S. Ganesan, F. Cicoira, C. M. Robertson, R. T. Oakley, F. Rosei and D. F. Perepichka, *Chem. Mater.*, 2008, **20**, 2484–2494.
- 19 W.-J. Liu, Y. Zhou, Y. Ma, Y. Cao, J. Wang and J. Pei, *Org. Lett.*, 2007, **9**, 4187–4190.
- 20 F. He, W. Wang, W. Chen, T. Xu, S. B. Darling, J. Strzalka, Y. Liu and L. Yu, *J. Am. Chem. Soc.*, 2011, **133**, 3284–3287.
- 21 J. A. A. W. Elemans, I. de Cat, H. Xu and S. de Feyter, *Chem. Soc. Rev.*, 2009, **38**, 722–736.
- 22 Y. Zhao and D. G. Truhlar, *Acc. Chem. Res.*, 2008, **41**, 157–167.
- 23 K. F. Dziubek and A. Katrusiak, *J. Phys. Chem. B*, 2008, **112**, 12001–12009.
- 24 O. Navon, J. Bernstein and V. Khodorkovsky, *Angew. Chem., Int. Ed. Engl.*, 1997, **36**, 601–603.
- 25 H. F. Lieberman, R. J. Davey and D. M. T. Newsham, *Chem. Mater.*, 2000, **12**, 490–494.
- 26 P. Politzer, J. S. Murray and T. Clark, *Phys. Chem. Chem. Phys.*, 2010, **12**, 7748–7757.